

Formation of targeted monovalent quantum dots by steric exclusion

Justin Farlow¹⁻³, Daeha Seo⁴⁻⁶, Kyle E Broaders¹, Marcus J Taylor⁷, Zev J Gartner¹⁻³ & Young-wook Jun⁴

Precise control over interfacial chemistry between nanoparticles and other materials remains a major challenge that limits broad application of nanotechnology in biology. To address this challenge, we used ‘steric exclusion’ to completely convert commercial quantum dots (QDs) into monovalent imaging probes by wrapping each QD with a functionalized oligonucleotide. We demonstrated the utility of these QDs as modular and nonperturbing imaging probes by tracking individual Notch receptors on live cells.

Commonly used strategies for chemically linking materials to nanoparticles result in products with valencies that follow a Poisson distribution owing to the presence of multiple reactive sites at the particle surface¹. For example, titration of QDs with increasing concentrations of a trithiolated DNA (ttDNA; **Fig. 1a**) generates an underdispersed Poisson distribution of product valencies², where the desired monovalent products are always obtained alongside unconjugated and multivalent QD byproducts (**Fig. 1b** and **Supplementary Fig. 1**). Multivalent nanoparticles present in these mixtures complicate the use of QDs for biological imaging because of the potential to perturb the function of their target by oligomerization, leading to receptor activation, internalization or redistribution on the cell surface³⁻⁵. This has motivated the development of methods for purifying monovalent nanoparticles from more complex mixtures⁵⁻⁹. However, the low synthetic yield obtained using these strategies, along with the multiple steps necessary to isolate pure monovalent products, have slowed broad application of QDs in the biomedical sciences. The aim of more recent efforts has been to synthesize QDs of controlled valency without the need for purification^{10,11} but these methods remain technically challenging for the typical researcher, have low product yield or lack modularity.

By nature of their large size, macromolecules or nanoparticles conjugated to QDs limit the maximum valency of products

by sterically excluding a large fraction of the QD surface from additional reactions^{10,12,13}. We envisioned adopting this concept to synthesize monovalent QDs (mQDs), in quantitative yield (>95%), by using a polymer with only a modest per-monomer affinity for the nanoparticle surface to wrap the QD in a single synthetic step, thus irreversibly forming a monovalent product and simultaneously preventing the binding of a second polymer molecule by ‘steric exclusion’ (**Fig. 1a**).

To implement this steric-exclusion strategy, we used phosphorothioate DNA (ptDNA) as a polymer because of the demonstrated affinity of phosphorothioates for semiconductor surfaces^{10,14}, the ease of synthesizing ptDNA of precisely defined sequence and length, and its commercial availability. After transfer of commercial CdSe:ZnS QDs from the organic to the aqueous phase, we treated the QDs with ptDNA of various sequences and lengths. Functionalization by negatively charged DNA produced QDs with an ionic character that were easily distinguishable from unfunctionalized QDs by agarose gel electrophoresis^{8,15}. We titrated QDs that emit at 605 nm (QD605) with increasing concentrations of an oligonucleotide comprising a 50-adenosine ptDNA domain (A₅₀^S, where ‘S’ refers to the sulfur atom in the phosphorothioate linkage) and a 20-nucleotide ssDNA targeting tail (**Fig. 1c**, **Supplementary Note 1**, and **Supplementary Figs. 1** and **2**). Agarose gel electrophoresis revealed a single band with increased mobility relative to starting materials, indicating production of a single species (**Fig. 1b**). At stoichiometric or higher ratios of ptDNA and QD, we observed no unfunctionalized or multiply functionalized products, consistent with the quantitative yield of mQDs (**Fig. 1c** and **Supplementary Figs. 1** and **3**). The strategy was also effective for generating mQDs of different sizes and shapes, and hence different emission spectra (**Fig. 1d**). QD-DNA conjugation was most efficient when we used oligonucleotides with a phosphorothioate backbone of adenosine bases (**Supplementary Fig. 4**).

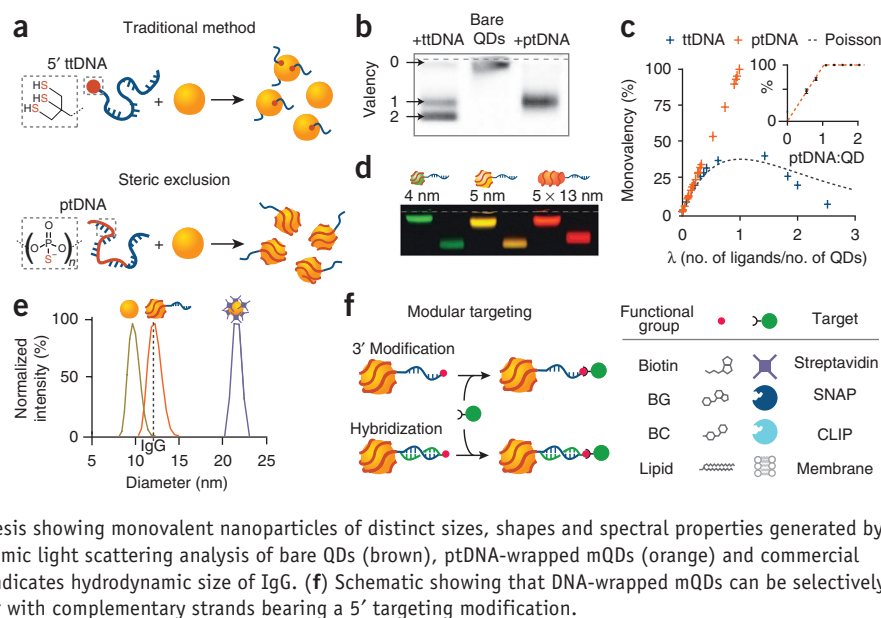
The ptDNA-wrapped mQDs had excellent colloidal and photo-physical properties in physiologically relevant buffers such as phosphate buffered saline (PBS) and culture medium when passivated with commercially available polyethylene glycol (PEG) ligands (**Supplementary Note 2**, **Supplementary Figs. 5-10** and **Supplementary Table 1**). As measured using dynamic light scattering, the hydrodynamic diameter of mQDs that emit at 605 nm was narrowly distributed around 12 nm, only 2 nm greater than that of bare particles (**Fig. 1e**). We investigated whether mQDs could be targeted to protein or lipid tags used frequently for live cell imaging. We achieved targeting by 3′ modification of the ptDNA or by hybridization of mQDs with complementary

¹Department of Pharmaceutical Chemistry, University of California San Francisco, San Francisco, California, USA. ²Tetrad Graduate Program, University of California San Francisco, San Francisco, California, USA. ³Center for Systems and Synthetic Biology, University of California San Francisco, San Francisco, California, USA.

⁴Department of Otolaryngology, University of California San Francisco, San Francisco, California, USA. ⁵Department of Chemistry, University of California Berkeley, Berkeley, California, USA. ⁶Materials Science Division, Lawrence Berkeley National Laboratory, Berkeley, California, USA. ⁷Department of Cellular and Molecular Pharmacology, University of California San Francisco, San Francisco, California, USA. Correspondence should be addressed to Z.J.G. (zev.gartner@ucsf.edu) or Y.J. (yjun@ohns.ucsf.edu).

Figure 1 | Exclusive synthesis of small, modular mQDs by the principle of steric exclusion.

(a) Schematic showing that incubation of bare QDs with ttDNA generates products with a distribution of valencies (top), whereas ptDNA molecules of appropriate size wrap the nanoparticle, preventing the reaction of a second strand owing to steric exclusion (bottom). (b) Agarose gel electrophoresis of reactions of ptDNA and ttDNA of identical length with bare nanoparticles optimized for yield of monovalent products. Dashed line indicates loading wells. (c) Average number of molecules bound per QD (λ) versus percentage of monovalent products using ttDNA and ptDNA. Dashed curve is fit with a Poisson distribution. Inset, reaction stoichiometry (ptDNA:QD) versus percentage of monovalent products. Error bars, s.d. ($n = 4$). Dashed orange line, fit with quantitative formation of mQDs. (d) Gel electrophoresis showing monovalent nanoparticles of distinct sizes, shapes and spectral properties generated by steric exclusion using 50-adenosine ptDNA. (e) Dynamic light scattering analysis of bare QDs (brown), ptDNA-wrapped mQDs (orange) and commercial streptavidin-conjugated Qdots (blue). Dashed line indicates hydrodynamic size of IgG. (f) Schematic showing that DNA-wrapped mQDs can be selectively targeted by 3' modification of the oligonucleotide or with complementary strands bearing a 5' targeting modification.



DNA bearing a 5' modification. We used these strategies to conjugate mQDs with biotin, benzylguanane (BG), benzylcytosine (BC) and lipids, thereby targeting them to streptavidin, SNAP tag, CLIP tag and cell membranes, respectively (Fig. 1f and Supplementary Figs. 11–13).

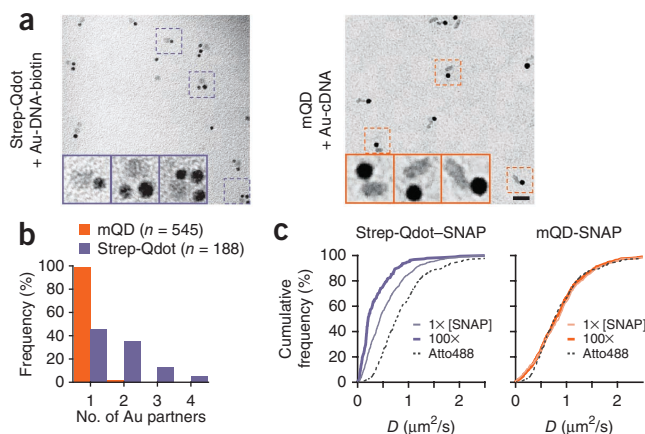
To provide more direct evidence for monovalency, we hybridized mQDs to gold nanocrystals bearing a single complementary sequence of single-stranded (ss)DNA. We observed the formation of a single higher-molecular-weight band by gel electrophoresis, consistent with the exclusive formation of heterodimers (Supplementary Fig. 14 and Supplementary Note 3). This band consisted nearly exclusively of mQD–Au heterodimers as revealed by transmission electron microscopy (TEM) (Fig. 2a,b). We rarely observed higher-order structures, such as trimers (2%) and tetramers (<0.2%) by TEM (Supplementary Fig. 15). In contrast, a reaction of commercial multivalent streptavidin-conjugated Qdots (Life Technologies) with similar DNA-linked monovalent gold nanocrystals conjugated to biotin resulted in multivalent products (Fig. 2a,b, Supplementary Fig. 14 and Supplementary Note 4).

To investigate whether mQDs alter the diffusion dynamics of their protein targets, we prepared supported lipid bilayers that incorporate a His-tagged SNAP protein via a small fraction of nickel

nitrilotriacetic acid–linked (Ni-NTA) lipid (Fig. 2c). We imaged the diffusion of this membrane-bound SNAP using a small organic dye, streptavidin-conjugated Qdots or mQDs (Supplementary Video 1 and Supplementary Note 4), and analyzed several hundred single-molecule trajectories for each probe. The diffusion coefficient measured using streptavidin-conjugated Qdots was significantly lower than using the dye ($P = 0.001$, nonparametric t test). The diffusion further slowed at greater SNAP protein density (Fig. 2c and Supplementary Fig. 16), consistent with the notion that multivalent QDs cross-link the target (Fig. 2c and Supplementary Figs. 17 and 18). In contrast, we observed a nearly identical distribution of diffusion coefficients for mQDs and the dye, independent of SNAP protein density (Fig. 2c). These data indicate that mQDs behave as bona fide and nonperturbing agents for single-molecule imaging in model cell membranes.

We next applied these small, modular mQDs to track individual Notch receptors on live cells. Activation of Notch has a central role in cell-fate decisions during development, normal tissue maintenance and cancer¹⁶, but little is known about the dynamics of Notch receptors at the cell surface. To track Notch, we inserted a sequence encoding a SNAP tag onto the 5' end of a previously reported human *NOTCH1* construct¹⁷ and expressed the resulting protein (SNAP-Notch) in U2OS cells (Supplementary Fig. 19).

Figure 2 | ptDNA-wrapped QDs are monovalent. (a) Representative TEM images of commercial streptavidin-conjugated Qdots (Strep-Qdot) incubated with gold nanoparticles bearing a biotinylated DNA sequence (left) and mQDs hybridized with gold nanoparticles bearing a complementary ssDNA sequence (cDNA, right). Insets, magnification of boxed regions, from left to right, respectively. Scale bar, 25 nm. (b) Frequency of QD valencies from TEM images of streptavidin-conjugated Qdots and mQDs. (c) Distribution of diffusion constants of SNAP proteins on supported lipid bilayers when probed with streptavidin-conjugated Qdots (Strep-Qdot–SNAP) and mQDs (mQD–SNAP). Thick lines are for data obtained with 100-fold greater protein concentration. (Thin purple line, $n = 756$, $0.56 \mu\text{m}^2/\text{s}$ mean; thick purple line, $n = 189$, $0.35 \mu\text{m}^2/\text{s}$ mean; thin orange line, $n = 490$, $0.89 \mu\text{m}^2/\text{s}$ mean; thick orange line, $n = 790$, $0.86 \mu\text{m}^2/\text{s}$ mean). The dotted black line shows diffusion measured with Atto488 ($n = 245$, $0.89 \mu\text{m}^2/\text{s}$ mean).



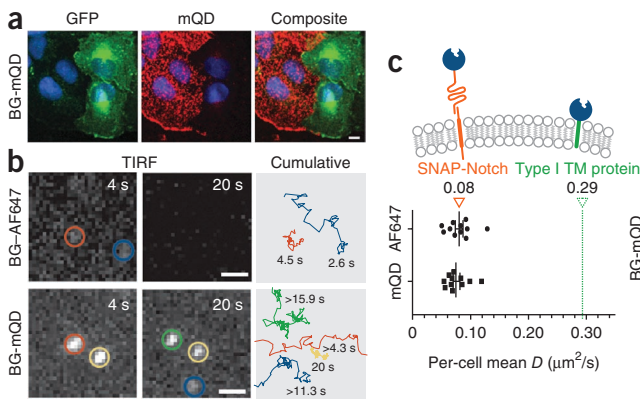


Figure 3 | Diffusion dynamics of SNAP-Notch proteins on surfaces of live cells. **(a)** Micrographs of cocultures of U2OS cells expressing either SNAP-Notch or Notch-GFP incubated with 1 μM BG-DNA and complementary mQDs that emit at 605 nm (red fluorescence). Scale bar, 10 μm . **(b)** Snapshots from the same region on the same cell showing trajectories of single SNAP-Notch proteins visualized by BG-Alexa Fluor 647 and BG-mQD. Scale bars, 1 μm . Complete trajectories are shown on the right. Some mQDs diffused in and out of the field of view. **(c)** Mean diffusion constant of at least 15 SNAP-Notch proteins per cell measured with both BG-mQDs or BG-Alexa Fluor dyes and of a SNAP protein fused to an unrelated type I transmembrane (TM) domain from CD86.

Note: Any Supplementary Information and Source Data files are available in the online version of the paper.

ACKNOWLEDGMENTS

We thank B. van Lengerich, L.D. Hughes and P. Haggie for assistance with single-particle-tracking software. S. Blacklow (Harvard University) provided human Notch1 constructs. R. Vale (University of California San Francisco) provided feedback on the single-molecule imaging. A.P. Alivisatos (University of California Berkeley) provided helpful discussion. J. Taunton and members of Cardiovascular Research Institute Core provided TIRF microscopes. N. Sturman helped with localization microscopy plugin. B. Liang, K. Southard and M. Todhunter generated some preliminary data. J.F. was supported by the University of California San Francisco Center for Synthetic and Systems Biology (P50 GM081879). D.S. was supported by Human Frontier Science Program Cross-disciplinary postdoc research fellowship. K.E.B. was supported by US National Institutes of Health National Research Service Award grant (5F32CA165620). Z.J.G. was supported by Kimmel Family Foundation. Y.J. was partly supported by 1R21EB015088-01 from the US National Institutes of Health NIBIB, and the Bryan Hemming Fellowship.

AUTHOR CONTRIBUTIONS

Z.J.G., J.F. and Y.J. conceived the study; J.F., Z.J.G. and Y.J. designed experiments; J.F., D.S., K.E.B., M.J.T., Z.J.G. and Y.J. performed experiments; J.F. and D.S. analyzed and interpreted the data; and J.F., Z.J.G. and Y.J. wrote the manuscript. All authors discussed and commented on the manuscript.

COMPETING FINANCIAL INTERESTS

The authors declare no competing financial interests.

Reprints and permissions information is available online at <http://www.nature.com/reprints/index.html>.

- Pons, T., Medintz, I.L., Wang, X., English, D.S. & Mattoussi, H. *J. Am. Chem. Soc.* **128**, 15324–15331 (2006).
- Shmueli, G., Minka, T.P., Kadane, J.B., Borle, S. & Boatwright, P. *J. R. Stat. Soc. Ser. C Appl. Stat.* **54**, 127–142 (2005).
- Saxton, M.J. & Jacobson, K. *Annu. Rev. Biophys. Biomol. Struct.* **26**, 373–399 (1997).
- Banerjee, D., Liu, A.P., Voss, N.R., Schmid, S.L. & Finn, M.G. *ChemBioChem* **11**, 1273–1279 (2010).
- Howarth, M. *et al. Nat. Methods* **5**, 397–399 (2008).
- Zanchet, D., Micheel, C.M., Parak, W.J., Gerion, D. & Alivisatos, A.P. *Nano Lett.* **1**, 32–35 (2001).
- Clarke, S. *et al. Nano Lett.* **10**, 2147–2154 (2010).
- Carstairs, H.M.J., Lymperopoulos, K., Kapanidis, A.N., Bath, J. & Turberfield, A.J. *ChemBioChem* **10**, 1781–1783 (2009).
- You, C. *et al. Angew. Chem. Int. Edn Engl.* **49**, 4108–4112 (2010).
- Tikhomirov, G. *et al. Nat. Nanotechnol.* **6**, 485–490 (2011).
- You, C. *et al. ACS Chem. Biol.* **8**, 320–326 (2013).
- Wilson, R., Chen, Y. & Aveyard, J. *Chem. Commun. (Camb.)* 1156–1157 (2004).
- Montenegro, J.-M. *et al. Adv. Drug Deliv. Rev.* **65**, 677–688 (2013).
- Jiang, L. *et al. Chem. Phys. Lett.* **380**, 29–33 (2003).
- Claridge, S.A., Liang, H.W., Basu, S.R., Fréchet, J.M.J. & Alivisatos, A.P. *Nano Lett.* **8**, 1202–1206 (2008).
- Bray, S.J. *Nat. Rev. Mol. Cell Biol.* **7**, 678–689 (2006).
- Gordon, W.R. *et al. Blood* **113**, 4381–4390 (2009).
- Douglass, A.D. & Vale, R.D. *Cell* **121**, 937–950 (2005).
- Triantafyllou, M., Morath, S., Mackie, A., Hartung, T. & Triantafyllou, K. *J. Cell Sci.* **117**, 4007–4014 (2004).
- Cairo, C.W. *et al. J. Biol. Chem.* **285**, 11392–11401 (2010).

The BG-mQDs labeled the cells expressing SNAP-Notch (red fluorescent cells) with high specificity. We observed negligible binding to cells expressing a control Notch-GFP construct lacking the SNAP tag (green fluorescent cells; **Fig. 3a** and **Supplementary Figs. 20** and **21**).

To confirm that the mQDs did not alter the mobility of Notch on live cells, we tracked SNAP-Notch labeled with mQDs and compared their average diffusion coefficients to those of receptors labeled with BG-Alexa Fluor 647 on the same cell (**Fig. 3b,c** and **Supplementary Video 2**). Analysis of mean square displacement versus time revealed mean diffusion coefficients (D) of $0.081 \mu\text{m}^2/\text{s}$ and $0.076 \mu\text{m}^2/\text{s}$ ($P = 0.7255$, nonparametric t test) for Notch imaged with Alexa Fluor 647 and mQDs, respectively. The measured diffusion constant for Notch deviates from those of other freely diffusing single-pass transmembrane proteins tracked by fluorescence microscopy (0.17 – $0.5 \mu\text{m}^2/\text{s}$)^{18,19}. The observed differences are not a consequence of cell type or imaging conditions, as a minimal protein based on the type I transmembrane domain from CD86 in U2OS cells also yielded an apparent diffusion coefficient ($0.29 \mu\text{m}^2/\text{s}$) several fold higher than that of Notch (**Fig. 3c**). In contrast, measured diffusion coefficients for Notch are consistent with reported values of single-pass transmembrane proteins known to interact with components of the cell surface or cell cortex^{18–20}. Although the physical source of the slow diffusion remains to be determined, our measurements suggest that the diffusion of Notch is dominated by interactions with proteins or glycans, rather than the viscous lipid bilayer.

In conclusion, we reported a potentially general method for preparing nanoparticles of fixed targeting valency using the principle of steric exclusion. The method is likely applicable to other nanoparticle materials using either modified nucleic acids or other polymers of low dispersity and controlled chemical functionality. mQDs prepared by steric exclusion retained their small size and excellent photophysical properties, and incorporated a single, modular targeting functionality. As a consequence of their monovalency, they do not perturb the diffusion of biomolecules in model membranes or live cells. The facile preparation of these small, bright, monovalent and modular imaging probes make them accessible to any researcher with basic molecular biology tools and reagents, and mQDs should find broad utility in studies requiring single-molecule imaging, either *in vitro* or in live cells.

METHODS

Methods and any associated references are available in the [online version of the paper](#).

ONLINE METHODS

Reagents. Reagents used were organic QDs (purchased from Invitrogen, Sigma-Aldrich or Ocean Nanotech Inc.; **Supplementary Fig. 22**), chloroform (ACROS, 99.8% purity), tetrabutylammonium bromide (TBAB, Sigma-Aldrich, 98.0%), 2,5,8,11,14,17,20-heptaoadocosane-22-thiol (mPEG thiol, Polypure, molecular weight (MW) 356.5 g/mol, 95% purity), HS-(CH₂)₁₁-(OCH₂CH₂)₆-OCH₂CO₂H (HSC₁₁EG₆CO₂H, ProChimia), streptavidin (Thermo Scientific), gold(III) chloride trihydrate (or hydrogen tetrachloroaurate, HAuCl₄•3H₂O, Aldrich, >99.9%), bis(p-sulfonatophenyl) phenylphosphine dehydrate dipotassium salt (BSPP, Aldrich, 97%), boric acid (Sigma-Aldrich, 99.5%), sodium hydroxide (ACROS, 99.0%), sodium chloride (NaCl, Sigma, 98%), Agarose LE (US Biotech Sources), Ficoll (Fisher BioReagents), Rhodamine 6G (R6G) and ethanol (Sigma-Aldrich). All reagents were used without further purification except QDs stabilized with amine ligands. These QDs were ligand-exchanged by reacting them with trioctylphosphine oxide (1 gram, Sigma-Aldrich, 90%) in CHCl₃ (10 ml) under inert atmosphere for 30 min. Gold nanoparticles (4 nm) were synthesized according to ref. 21, and then conjugated with ssDNA (5'-trithiol-(GTCA)₅). Singly modified gold-DNA nanoparticles were purified according to ref. 6.

Instruments and characterization. Measurements of dynamic light scattering were performed with a Malvern Zetasizer Nano zs90. Transmission electron microscopy images were taken using a Tecnai G220 S-TWIN at an acceleration voltage of 200 kV. Flow cytometry was performed on a BD FACSCalibur and FACSaria II. Total internal reflected fluorescence (TIRF) microscopy was performed on a Nikon Eclipse TI. Confocal microscopy was carried out on a Zeiss Axio Observer Z1. Absorption spectra of QDs were obtained with either Shimadzu UV-1650 PC or HP8453. The quantum yield of QDs (Φ_x) was measured by a FP-6500 (Jasco) spectrofluorometer with 490-nm excitation following the method in ref. 22

$$\Phi_x = \Phi_{st}(F_x f_{st}(\lambda_{ex}) n_x^2) / (F_{st} f_x(\lambda_{ex}) n_{st}^2)$$

where Φ_{st} is fluorescence quantum yield of a dye (R6G) using the reported value of 0.95 in ethanol, and used as a reference, F is the integrated emission spectrum, $f(\lambda_{ex})$ is the absorption factor given by $f_x(\lambda_{ex}) = 1 - 10^{-A(\lambda_{ex})}$ ($A(\lambda_{ex})$ is an absorbance at the excitation wavelength) and n is the refractive index of medium (1.313 for water and 1.360 for ethanol).

Statistical analyses. All P values were calculated by nonparametric t test with GraphPad Prism version 6.00 (GraphPad Software) via the Mann-Whitney method.

Synthesis of phosphorothioate oligonucleotides. Oligonucleotides were synthesized using an Expedite DNA synthesizer by standard phosphoramidite chemistry and deprotected for 15 min at 65 °C using 50:50 ammonium hydroxide:methylamine (AMA). Phosphoramidites and synthesis reagents were purchased from Glen Research and AZCO Biotechnology. Phosphorothioate-containing oligonucleotides were synthesized by replacing the standard oxidizing solution with 1% DDTT

(3-((dimethylamino-methylidene)amino)-3H-1,2,4-dithiazole-3-thione; Glen Research) dissolved in 60:40 pyridine:acetonitrile, and were prepared DMT(dimethoxytrityl)-ON. All oligonucleotides were purified using an Agilent 1200 HPLC equipped with Zorbax XDB-C8 semi-preparative column running an acetonitrile and 0.1 M TEAA (triethylamine acetate) mobile phase. Purified phosphorothioate-containing oligonucleotides retained the 5'-DMT protecting group, and were used without further modification after lyophilization. Sequences of oligonucleotides used in this study are summarized in **Supplementary Table 2**.

Phase transfer of organic QDs into aqueous phase. To organic QDs (3.0 ml in chloroform), TBAB (2.0 ml, 0.3 M in chloroform) and mPEG thiol (180 μ l) were added. After 30 min, aqueous NaOH (4.0 ml, 0.2 M) was added to this mixture. The mixture was briefly vortexed and centrifuged at 1,000g for 30 s to completely separate the phases. The aqueous layer was recovered, and the collected QDs were concentrated using a centrifugal (30 kDa, Amicon) device, and then buffer exchanged by NAP desalting column (GE Healthcare) into 10 mM Tris containing 30 mM NaCl (pH 8) as an eluent. QD concentration was determined by absorbance at 350 nm (extinction coefficients of QDs that emit at 545 nm, 585 nm and 605 nm are 1,590,000 M⁻¹ cm⁻¹, 3,500,000 M⁻¹ cm⁻¹ and 4,400,000 M⁻¹ cm⁻¹, respectively).

Preparation of ptDNA-mQDs. To confirm the exact 1:1 stoichiometry of DNA versus QDs, we first added 0.5 equivalents of ptDNA (100 nM, 0.5 ml) to QDs (100 nM, 1 ml), drop-wise under vigorous stirring. We found that drop-wise addition is critical for exclusive formation of mQDs (**Supplementary Fig. 23**). After 9 h of reaction, the extent of DNA conjugation to QDs was confirmed by electrophoresis using Mini-Sub Cell GT cell (Bio-Rad) with 0.8% Superpure agarose (US Biotech Sources) in sodium borate buffer at 8 V/cm for 15 min. The conjugation yield was determined by relative fluorescence intensity between two bands on an agarose gel corresponding to bare mQDs. We then added an appropriate amount of ptDNA solution (based on the above calculation), and the mixture was further reacted for 9 h. For further reactions with biomolecules or cell-surface receptors, the surface ligands were exchanged with HSC₁₁H₂₂(OCH₂CH₂)₆OCH₂CO₂H ($\times 10^4$ equivalents of QDs) for 10 min. The resulting solution was concentrated to 0.2 ml and then desalted with a NAP-10 column before use. No noticeable aggregation of QDs after DNA conjugation was observed (**Supplementary Fig. 24**).

Modular conjugation of mQDs. mQD- X (where X is biotin, BG or BC). Biofunctional moieties can be easily added to mQDs either by directly incorporating a desired functional group (e.g., biotin) at the 3'-end of DNA to be conjugated or by incorporation into the complementary strand (e.g., BG-DNA, BC-DNA). Hybridization reactions were performed as follows: to a solution containing mQDs bearing (ACTG)₅ tail, 500 μ l of a 50 nM solution in 10 mM Tris and 100 mM NaCl were added to 10 equivalents of X-(CAGT)₅ (25 μ M, 10 μ l). After 6 h, excess complementary DNAs were removed by a centrifugal filter device (molecular weight cutoff (MWCO), 30 kDa, Amicon). The functionality of the mQD- X molecules was confirmed by incubating ten equivalents of target biomolecules (streptavidin, SNAP or CLIP)

at 4 °C for 5 h. Quantitative reaction was confirmed by agarose gel electrophoresis.

QD-Au hybridization. mQDs bearing a (CAGT)₅ tail were treated with 10 equivalents of Au nanoparticles bearing a single complementary sequence of ssDNA in Tris buffer (10 mM Tris 200 mM NaCl, pH 8). Separately, streptavidin-conjugated Qdots (Life Technologies, Qdot 605 Streptavidin Conjugate) were treated with 10 equivalents of Au nanoparticles bearing a single biotinylated ssDNA under the same reaction conditions. Monovalent Au nanoparticles were synthesized via published methods⁶ and surface-modified with either HS-C₃H₇(OCH₂CH₂)₆OCH₃ (mPEG-SH) or HS-C₃H₇(OCH₂CH₂)₆OCH₂-COOH (COOH-PEG-SH). After overnight reaction, the coupling efficiency was determined by an agarose gel electrophoresis using Mini-Sub Cell GT Cell (Bio-Rad) with 2% Superpure agarose (US Biotech Sources) in sodium borate buffer at 10 V/cm for 20 min. Bands exhibiting both gold color and QD fluorescence were extracted via electro dialysis and then drop-casted onto a carbon-coated copper TEM grid for imaging. Statistical analysis of QD valency was performed by counting the number of gold nanocrystals per QD (Supplementary Fig. 15).

Imaging SNAP-protein diffusion in supported lipid bilayers. Small unilamellar vesicles containing 97.5% 1,2-dioleoyl-3-sn-phosphatidylethanolamine (DOPE), 2% 1,2-dioleoyl-sn-glycero-3-((N-(5-amino-1-carboxypentyl)-iminodiacetic acid)succinyl)nickel (DGS-Ni-NTA) and 0.5% 1,2-dioleoyl-sn-glycero-3-phosphoethanolamine-N-(methoxy(polyethylene glycol)-5000) (ammonium salt) were deposited onto well-cleaned glass surfaces. Surfaces were washed with PBS containing 1% BSA, then incubated with DNA-linked SNAP protein; 5 μM 10× His-tagged SNAP dyed with NHS-Atto488 incubated with 5 μM BG-DNA (BG-(CAGT)₅) for 30 min at room temperature. Surfaces were further washed and then incubated with either mQDs bearing (CT)₁₀(ACTG)₅ or biotin-DNA (biotin-(CT)₁₀(ACTG)₅) followed by streptavidin-conjugated Qdots. Surfaces were imaged at 32 °C in TIRF mode with a 100× objective lens using either a 405-nm or 491-nm laser at 20 Hz on a Hamamatsu Imagem EM electron-multiplying charge-coupled device (EM-CCD).

Cloning and cell lines. *SNAP-Notch* was constructed by inserting the sequence encoding the SNAP tag (NEB) between the Flag tag sequence and the Notch sequence of the *Notch-Gal4* construct (gift from S. Blacklow, Harvard University). U2OS cells containing *Notch-GFP* in pcDNA6 along with a U2OS Flp-In line containing the Tet repressor were also gifts from S. Blacklow. *SNAP-Notch* was 'flipped' into the U2OS cell line per Invitrogen's protocol; briefly, cells were cotransfected with a plasmid encoding Flp recombinase (pOG44) and the above *SNAP-Notch* construct using Lipofectamine 2000 followed by selection with 400 μg/ml hygromycin for 10 d. Cells were cultured in McCoy's 5A medium with 10% FBS and passaged every 3–4 d. Jurkat cells were cultured in RPMI containing HEPES

and 10% FBS. All cells were maintained at 37 °C and in 5% CO₂ in a humidified incubator.

Live-cell labeling and imaging. Unless otherwise noted, cells were incubated with 1 μM BG-DNA for 30 min at 37 °C, washed three times with PBS containing 1% BSA and then incubated with 200 pM mQDs for 5 min at room temperature before a final wash with 1% BSA. In dye-comparison experiments, cells were incubated simultaneously with 1 μM BG-DNA and 0.2 μM BG-Alexa Fluor 647 (Surface-SNAP-647, NEB). For single-particle tracking, mQDs were incubated in PBS containing 1% BSA for 30 min at room temperature before being added to cells at a concentration of 0.2 nM. For high-density labeling, mQDs were incubated in 5% alkali-soluble casein (EMD Millipore) before being added to cells at a concentration of 5 nM. Live cells were imaged on a Ti Nikon Eclipse inverted microscope (use courtesy of the UCSF Cardiovascular Research Institute) at 37 °C with 5% CO₂. Two 30-s movies were acquired in sequence at 20 Hz; first with dye, and then with mQDs. QDs were imaged using a 488-nm laser from an Agilent Technologies MLC 400B.

Flow cytometry. Jurkat cells were labeled with DNA according to a published procedure²³. Briefly, cells were incubated for 5 min at room temperature with 5.5 μM of a lipid-DNA sequence identical or complementary to that on the QDs. Cells were washed 3× with PBS containing 1% BSA and then incubated with 5 nM mQDs for 5 min at room temperature before additional washing. Cells were then analyzed using a BD FACSAria flow cytometer using the 405-nm laser coupled with a 610/20 nm filter set.

High-density labeling of cells with dyes and QDs. Both SNAP-Notch and Notch-GFP expressing cells were cocultured in 8-well chamber slides for 48 h in the presence of 1 μg/ml doxycycline. For high-density mQD labeling, cells were fixed using 5% formaldehyde and then immediately imaged via confocal microscopy. QDs were excited using a 405-nm laser. Nuclei were stained with either DAPI when Notch was visualized using Alexa Fluor 647, or with DRAQ5 when using QDs, as DAPI fluorescence bleeds into the QD channel.

Background binding measurements. For low-density (200 pM) signal-to-noise ratio (S/N) measurements, images were obtained under single-particle tracking conditions on a TIRF microscope, but with exposures of 1 s rather than 0.05 s. For high-density (5 nM) S/N measurements, images were obtained from fixed samples on a confocal microscope. QDs in comparable regions of interest on both 'green' and 'non-green' cells were counted using the 'Localization Microscopy' plugin in μManager. At least 120 1,089 μm² regions of interest across two labeling experiments and ten different fields were used to calculate S/N.

21. Jana, N.R., Gearheart, L. & Murphy, C.J. *Langmuir* **17**, 6782–6786 (2001).

22. Grabolle, M. *et al. Anal. Chem.* **81**, 6285–6294 (2009).

23. Selden, N.S. *et al. J. Am. Chem. Soc.* **134**, 765–768 (2012).